Pergamon

Int. J. Solids Structures Vol. 32, No. 17/18, pp. 2751–2778, 1995

0020-7683/95 $9.50 + .00

0020-7683(94)00294-0

ON SHEAR FLOW LOCALIZATION WITH TRACTION-CONTROLLED BOUNDARIES

TAREK G. SHAWKI
Department of Theoretical and Applied Mechanics, University of Illinois at Urbana-Champaign, Urbana, IL 61801, U.S.A.

(*Received* 3 *February* 1994)

Abstract— The interactive roles of inertia and material viscosity as regards the evolution of inhomogeneous plastic flow are analyzed. The analysis is presented in the context of the dynamic, one-dimensional simple shear of a thermo-viscoplastic material subjected to traction-controlled boundaries. Existence and uniqueness questions of an exact homogeneous solution for this initial boundary-value problem are investigated. The breakdown of the so-called quasi-static homogeneous solution is related to the onset of localization. We introduce a dimensionless number, called the deformation number, and denoted by R_D, as the ratio of inertial to viscous stresses. Characterization of a given deformation as being dynamic is shown to be related to large values of R_D instead of simply high rates of applied loading. A model problem is formulated in order to illustrate the basic features of solutions for this class of deformations. An exact solution is derived for the model problem as well as a solution based on matched asymptotic expansions. It is shown, based on the model problem and fully non-linear finite difference solutions, that plastic deformation localizes within narrow bands in the neighborhood of the boundaries. The shear band thickness is inversely proportional to the square root of the deformation number. The role of material viscosity concerning the introduction of a length scale to dynamic deformations of rate-dependent solids is illustrated.

1. INTRODUCTION

Evolution of inhomogeneous deformation patterns in which plastic flow localizes within narrow bands, commonly referred to as shear bands, has received the attention of extensive research efforts in the past two decades. The connection between the evolution and subsequent intensification of inhomogeneous plastic flow and catastrophic structural failure explains the technical interest in the phenomenon of shear flow localization. The name shear localization derives from the observation that the primary deformation mode within the regions of localized plastic deformation is that of one-dimensional simple shear. Shawki and Clifton (1989) have presented an extensive study of various aspects of shear band formation in thermal viscoplastic materials as well as a review of the recent analyses concerning the phenomenon of shear strain localization. Most of these analyses were concerned with the critical conditions associated with the onset of shear flow localization. The primary difficulty associated with such studies may be attributed to the wide spectrum of materials, loading conditions, observation scales and rates of deformation at which shear localization takes place. Our limited ability as regards the characterization of the material response over several decades of temperature, strain rate and strain poses a serious difficulty to such analytical attempts that aim at improving our understanding of shear flow localization. A variety of mechanisms have been suggested for the analysis of shear flow localization. The success of a given mechanism depends on how closely it simulates the deformation conditions at hand. Two major assumptions have been used extensively by several authors for the analysis of shear flow localization: (i) quasi-static deformation conditions and/or (ii) rate-independent material response. The first assumption implies that inertial effects are assumed to be "sufficiently small" throughout the deformation whereas the second assumption implies that the material considered exhibits a negligible strain rate dependence. Table 1 summarizes the mathematical notions of shear localization in four possible frameworks employing the above assumptions.

Table 1. Frameworks for the analysis of shear flow localization

	Viscous effects	
Inertia effects	Rate-independent material response	Rate-dependent material response
Quasi-static deformations	Loss of ellipticity	Unbounded solutions
Dynamic deformations	Loss of hyperbolicity	Bounded solution evolution

Rudnicki and Rice (1975) and Rice (1977) have presented the general mathematical theory for the analysis of shear localization in rate-independent materials which are deforming quasi-statically and isothermally. In the former theory, the onset of localization is viewed as a material instability that takes place when the velocity equations of continuing equilibrium suffer a *loss of ellipticity*. In Section 2, we present a brief discussion concerning the governing equations for the dynamic, one-dimensional simple shearing deformation of a thermally-sensitive, viscoplastic material subject to traction-controlled boundaries. We also present a graphical tool that is useful for the presentation of the material response throughout the deformation history as well as being useful in interpreting future results. In Section 3, we examine the questions of existence and uniqueness of a spatially-independent solution to the considered initial boundary-value problem in the two cases corresponding to large and small inertial effects. In Section 4, we examine the intimate relationship between the failure of the quasi-static, approximate homogeneous solution and the onset of shear strain localization. This feature is a key to our future developments. In Sections 5 and 6, we present several attempts at improving understanding of the evolution of inhomogeneous deformation fields as soon as inertial effects become significant. The structure of the narrow regions in which plastic deformation localizes is examined thoroughly. In Section 7, we present an exact, closed-form solution for the dynamic simple shearing of a material described by a Kelvin–Voigt model. This solution illustrates several important features regarding the phenomenon of shear localization and sets the stage for the fully non-linear solutions in Section 8 and the discussion in Section 9 where we introduce a dimensionless number, called the deformation number, which is an exact analogue to the Reynold's number used in studies of viscous fluid flow.

Dynamic deformations are tied to large values of the deformation number instead of merely high rates of deformation. An expression for shear band thickness is introduced. This discussion illustrates the interactive roles of inertia and material rate sensitivity as regards the introduction of a viscous length scale to the problem. Difficulties associated with the quasi-static and/or the rate-independent limits are clearly illustrated and rationalized.

2. PROBLEM FORMULATION

Consider the simple shearing motion of a material slab whose cross-section occupies the x–y plane as illustrated in Fig. 1. The slab has a finite thickness H in the x direction while it extends indefinitely in the y and z directions. Shear traction histories are prescribed at the two boundaries corresponding to $x = 0$ and $x = H$.

We further assume that all physical quantities are uniform in both the y and z directions so that the deformation depends only on the single space coordinate, x. Under these conditions the only non-zero stress components are $\sigma_{xy} \equiv \tau$, σ_{yy}, σ_{xx} and σ_{zz}. Hence, the equations governing the considered one-dimensional simple shear are given by [see Shawki and Clifton (1989) for further details]:

$$\rho v_{,t} = \tau_{,x} \tag{1a}$$

$$v_{,x} = \dot{\gamma}^p + \mu^{-1}\tau_{,t} \tag{1b}$$

$$\theta_{,t} = r_0\theta_{,xx} + r_1\tau\dot{\gamma}^p \tag{1c}$$

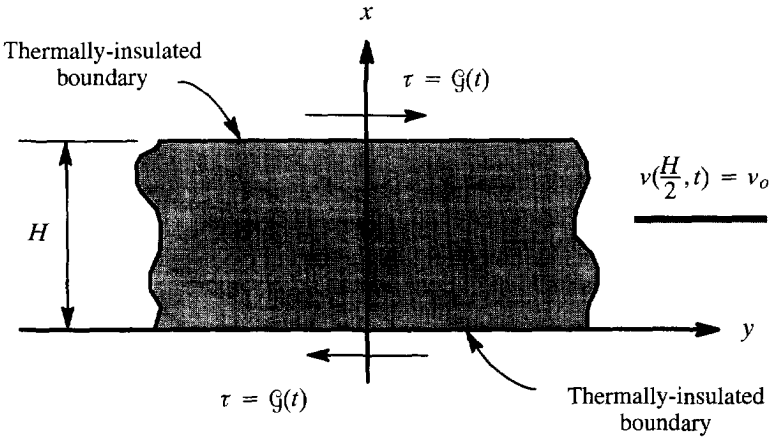

Fig. 1. A schematic of traction-controlled simple shear.

$$\tau = f(\dot{\gamma}^p, \theta, \gamma^p) \quad \text{or} \quad \phi = g(\tau, \theta, \gamma^p), \tag{1d}$$

where

$$\phi \equiv \frac{\partial \gamma^p}{\partial t} \quad \text{and} \quad \gamma^p(x, t) = \gamma^p(x, t_0) + \int_{t_0}^{t} \phi(x, \eta)\, \mathrm{d}\eta. \tag{1e}$$

The foregoing equations represent the balance of linear momentum (1a), the additive decomposition of the total strain rate into elastic and viscoplastic contributions (1b), the energy balance (1c) and the material behavior description (1d). Here, ρ is the mass density, $v(x, t)$ the particle velocity in the y direction, $\tau(x, t)$ the shear stress, $\phi(x, t)$ the plastic strain rate, μ the shear modulus of elasticity, $\theta(x, t)$ the absolute temperature, $r_0 \equiv \kappa/C$ where κ denotes the material thermal conductivity and C denotes the specific heat per unit mass, $r_1 \equiv \beta/C$ where β denotes the amount of plastic work that is converted to heat (which typically assumes a value like 0.9). Equations (1d) are two alternative expressions of the material's thermal-viscoplastic response.

It should be noted that eqns (1a–e) remain valid for arbitrarily large deformations. Insight into thermoplastic instability obtained from the study of eqns (1a–e) is expected to be applicable to the understanding of shear strain localization in a wide class of materials. Further, we define the following measures for the material various sensitivities:

$$S_1 \equiv \frac{\partial f}{\partial \phi}, \quad S_2 \equiv \frac{\partial f}{\partial \theta}, \quad S_3 \equiv \frac{\partial f}{\partial \gamma^p}. \tag{2}$$

The above measures may be viewed as the components of a vector $\mathbf{S} \equiv (S_1, S_2, S_3)^{\mathrm{T}}$ relative to a Cartesian reference frame whose unit vectors are denoted by $\mathbf{e}_1$, $\mathbf{e}_2$ and $\mathbf{e}_3$, respectively (see Fig. 2). If we further define the vector $\mathbf{z} \equiv (\phi, \theta, \gamma^p)^{\mathrm{T}}$, then the incremental change in the flow stress can be expressed as follows

$$\mathrm{d}\tau = \mathbf{S} \cdot \mathrm{d}\mathbf{z} = S_1\, \mathrm{d}\phi + S_2\, \mathrm{d}\theta + S_3\, \mathrm{d}\gamma^p. \tag{3}$$

The function S_1 represents strain rate sensitivity and it is assumed positive in our subsequent discussions. The function S_2 represents thermal softening ($S_2 < 0$) or thermal hardening ($S_2 > 0$). The function S_3 represents strain hardening ($S_3 > 0$) or strain softening ($S_3 < 0$). Figure 2 illustrates special cases of interest. For a given material description, the material behavior, at a fixed position x and fixed time t, is described by a position vector $\mathbf{S}$ in the three-dimensional space (S_1, S_2, S_3). The planes Π_1, Π_2 and Π_3 are described by their unit normals $(1, 0, 0)^{\mathrm{T}}$, $(0, 1, 0)^{\mathrm{T}}$ and $(0, 0, 1)^{\mathrm{T}}$, respectively. Vectors $\mathbf{S}$ that lie in the planes Π_1

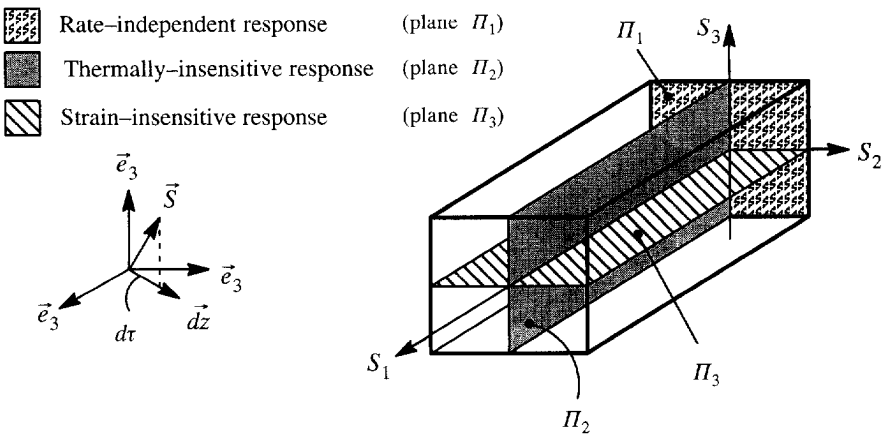

Fig. 2. The material response space.

(Π_2 or Π_3) correspond to the cases of rate-independent material response (thermally-insensitive response or strain-insensitive response).

In this work, we will be concerned with materials for which

$$S_1 \geqslant 0, \quad S_2 \leqslant 0, \quad S_3 \geqslant 0, \tag{4}$$

i.e. we consider materials exhibiting strain rate hardening, thermal softening and strain hardening. Graphically, such materials will be characterized by vectors **S** occupying the upper left parallelepiped region of our proposed material response space. Such material response will be referred to as a thermal-viscoplastic response. It is important to note that the measures S_k, $k = 1, 2, 3$ depend, in general, on the solution to the considered initial boundary-value problem and hence on the independent variables x and t. For a fixed position $x = x_0$, the temporal evolution of the three measures S_k traces a space curve Γ_0 in the material response space. The collection of such traces for all positions $x \in [0,1]$ describes a material response surface φ in the considered space. Examination of this surface provides useful insights regarding the material response during various stages of shear band evolution.

Furthermore, it is convenient to express the system (1) of governing equations in a dimensionless form. The dimensionless quantities are defined as follows:

$$\hat{t} = \frac{t}{t_0}, \quad \hat{\tau} = \frac{\tau}{\tau_0}, \quad \hat{v} = \frac{v}{H/t_0}, \quad \hat{\phi} = \frac{\phi}{\phi_0}, \quad \hat{\mu} = \frac{\mu}{\tau_0}, \quad \hat{\theta} = \frac{\theta}{\theta_0},$$
$$\hat{r}_0 = \frac{r_0 t_0}{H^2}, \quad \hat{r}_1 = \frac{r_1 \tau_0}{\theta_0}, \quad \hat{\rho} = \frac{\rho H^2}{\tau_0 t_0^2},$$
$$\hat{S}_1 = \frac{S_1 \phi_0}{\tau_0}, \quad \hat{S}_2 = \frac{S_2 \theta_0}{\tau_0}, \quad \hat{S}_3 = \frac{S_3}{\tau_0}. \tag{5}$$

The subscript zero denotes appropriately selected reference quantities while the characteristic time $t_0 = 1/\phi_0$ is the time required to obtain a unit shear strain at the nominal strain rate ϕ_0. The above dimensionless quantities are selected such that the governing system of eqns (1a–e) remains unchanged once they are introduced. We will assume the dimensionless form in our subsequent discussions. Moreover, the superposed "hat" is dropped for convenience of notation.

Complete description of the problem requires the prescription of appropriate initial and boundary conditions. Such auxiliary conditions consist of the *homogeneous* initial data

$$v(x,0) = x, \quad \gamma^p(x,0) = \gamma_0 \qquad (6)$$
$$\phi(x,0) = \sigma(x,0) = \theta(x,0) = 1$$

as well as the following boundary conditions:

$$\tau(0,t) = \tau(1,t) = \mathscr{G}(t) \qquad (7a)$$

and

$$\frac{\partial\theta}{\partial x}(0,t) = \frac{\partial\theta}{\partial x}(1,t) = 0. \qquad (7b)$$

In eqns (6), the initial strain γ_0 is a constant while we note that $f(1,1,\gamma_0) = 1$. Moreover, the function $\mathscr{G}(t)$ in eqn (7a) is a prescribed function that satisfies $\mathscr{G}(0) = 1$ in order to be consistent with the initial data for the flow stress. The above conditions imply that we are concerned with the dynamic simple shearing deformation from an initially homogeneous state with thermally-insulated and stress-controlled boundaries.

3. EXISTENCE AND UNIQUENESS OF A HOMOGENEOUS SOLUTION

In this section, we examine the questions of existence and uniqueness in relation to solutions of the posed initial boundary-value problem described by eqns (1a–e) and the auxiliary conditions (6) and (7). We seek a homogeneous (spatially-independent) solution of the form

$$\gamma^p(x,t) = \bar{\gamma}(t), \quad \theta(x,t) = \bar{\theta}(t), \quad \tau(x,t) = \bar{\tau}(t). \qquad (8a)$$

Making use of eqn (1b), the consistent velocity profile must have the form

$$\bar{v}(x,t) = \alpha(t)x + \zeta(t), \quad 0 \leqslant x \leqslant 1. \qquad (8b)$$

We further require the velocity distribution to be anti-symmetric about the central position $x = 0.5$ by enforcing that $v(0.5,t) = 0.5$. This requirement leads to the relation $2\zeta(t) = 1-\alpha(t)$ which reduces the form (8b) to

$$\bar{v}(x,t) = \alpha(t)(x-\tfrac{1}{2}) + \tfrac{1}{2}, \quad 0 \leqslant x \leqslant 1, \qquad (9)$$

with the further restriction that $\alpha(0) = 1$ for consistency with the initial data for the particle velocity.

Now, we distinguish the three important deformation classifications illustrated in Table 2. Note that the distinction between the three deformation classifications is related to the "size" of the inertia term (which can be equivalently achieved in terms of the stress gradient [see eqn (1a)]. In other words, we may recognize the case of a static deformation as that in which the flow stress is spatially uniform, the quasi-static deformation as that in which the flow stress exhibits *weak* spatial dependence and the dynamic deformation as that in which the flow stress depends strongly on x. Furthermore, it is important to emphasize that the quasi-static approximation is viewed as appropriate when the inertia is *sufficiently small* or, alternatively, as the mathematical limit $\rho \to 0$ in eqn (1a). This implies

Table 2. Inertial deformation classifications

Deformation	Static	Quasi-static	Dynamic
Mathematical characterization	$\rho\frac{\partial v}{\partial t} = 0$	$\rho\frac{\partial v}{\partial t} \approx 0$	$\rho\frac{\partial v}{\partial t}$ finite

that the particle velocity may still be time-dependent provided that the inertia term remains sufficiently small. Consequences of this classification are discussed thoroughly in this work.

3.1. *Dynamic deformation*

Substitution of eqn (9) and the homogeneous form of the flow stress in eqn (1a) gives $\alpha(t) = \alpha(0) = 1$ which yields the homogeneous velocity profile $\bar{v}(x, t) = x$ as well as the homogeneous stress profile $\bar{\tau}(x,t) = \mathscr{G}(t)$. Equation (1b) provides the homogeneous plastic strain rate $\dot{\bar{\phi}}(t) = 1 - [\dot{\mathscr{G}}(t)/\mu]$. Equation (1e) gives the homogeneous plastic strain whereas the energy equation (1c) yields the homogeneous temperature. The complete homogeneous solution is given by

$$\bar{v}(x, t) = x, \quad \bar{\tau}(t) = \mathscr{G}(t), \quad \bar{\phi}(t) = 1 - \left(\frac{\dot{\mathscr{G}}(t)}{\mu}\right) \tag{10a}$$

$$\bar{\gamma}(t) = (\gamma_0 + t) - \left\{\frac{\mathscr{G}(t) - 1}{\mu}\right\} \tag{10b}$$

$$\bar{\theta}(t) = 1 - \frac{r_1}{2\mu}[\mathscr{G}^2(t) - 1] + r_1 \int_0^t \mathscr{G}(\eta)\, \mathrm{d}\eta. \tag{10c}$$

Substitution of the above solution in eqn (1d) gives the consistency requirement:

$$\mathscr{G}(t) = f(\bar{\phi}(t), \bar{\theta}(t), \bar{\gamma}(t)). \tag{11}$$

Equation (11) is a non-linear ordinary differential equation for the boundary traction history $\mathscr{G}(t)$. It is evident that the requirement (11) is not satisfied for arbitrary functions $\mathscr{G}(t)$ and general material descriptions f. Hence, we conclude that the dynamic simple shearing deformation of a thermal-viscoplastic solid subject to prescribed stresses at the insulated boundaries is always inhomogeneous, i.e. there exists no homogeneous solution for the considered problem.

3.2. *The quasi-static approximation*

In this case, the homogeneous solution for the flow stress is still given by the second of eqns (10a) while we satisfy the equation of motion (1a) by considering the mathematical limit $\rho \to 0$ which allows the function $\alpha(t)$ in eqn (9) to be time-dependent. Equations (1c) and (1d) can be used to provide the following initial-value problem, described by a system of non-linear, non-autonomous ordinary differential equations, for the homogeneous solution:

$$\frac{\mathrm{d}\bar{\theta}(t)}{\mathrm{d}t} = r_1 \mathscr{G}(t) g(\mathscr{G}(t), \bar{\theta}(t), \bar{\gamma}(t)) \equiv h_1(\bar{\theta}, \bar{\gamma}, t), \quad \bar{\theta}(0) = 1, \tag{12a}$$

$$\frac{\mathrm{d}\bar{\gamma}(t)}{\mathrm{d}t} = g(\mathscr{G}(t), \bar{\theta}(t), \bar{\gamma}(t)) \equiv h_2(\bar{\theta}, \bar{\gamma}, t), \quad \bar{\gamma}(0) = \gamma_0. \tag{12b}$$

The above initial-value problem may be expressed in the vector form

$$\frac{\mathrm{d}\mathbf{a}(t)}{\mathrm{d}t} = \mathbf{h}(\mathbf{a}, t), \quad \mathbf{a}(0) = (1, \gamma_0)^{\mathrm{T}}, \tag{13a}$$

where

$$\mathbf{a}(t) = (\bar{\theta}(t), \bar{\gamma}(t))^{\mathrm{T}} \quad \text{and} \quad \mathbf{h}(\mathbf{a}, t) \equiv (h_1(\mathbf{a}, t), h_2(\mathbf{a}, t))^{\mathrm{T}}. \tag{13b}$$

Sufficient conditions for the local existence, uniqueness and well-posedness of solutions to the non-linear initial-value problem (13) require that the function $\mathbf{h}(\mathbf{a},t)$ be continuous and that it satisfies a Lipschitz continuity condition with respect to $\mathbf{a}$ in an open connected set $D \in R \times R^n$ with the requirement $\{\mathbf{a}(0),0\} \in D$; see, for example, Coddington and Levinson (1955). We will consider the class of materials, i.e. the functions f and g in eqn (1d), for which those sufficient conditions are met. Hence, a unique, well-posed solution $\mathbf{a}(t)$ of the system (13) exists. Using the foregoing solution, one can readily calculate the time-dependent function $\alpha(t)$ appearing in eqn (9) from

$$\alpha(t) = \frac{\mathrm{d}\bar{\gamma}(t)}{\mathrm{d}t} + \frac{\dot{\mathscr{G}}(t)}{\mu}. \tag{14}$$

The temporal dependence of $\alpha(t)$ causes the particle velocity to be time-dependent and, therefore, the inertia term $I(t) \equiv \rho\, \partial v/\partial t$ to be non-zero. Hence, this solution should only be viewed as an *approximation* that remains valid as long as the inertia term remains sufficiently small.

4. FAILURE OF THE QUASI-STATIC APPROXIMATION

The quasi-static solution obtained by solving the initial-value problem (13) is attractive for various analyses concerning shear localization because it offers an exact solution to the non-linear problem described by eqns (1a–e). Molinari and Clifton (1987) and Shawki and Clifton (1989) have presented several quasi-static solutions for a number of material descriptions. Those solutions proved useful regarding the improved understanding of plastic flow localization. Molinari and Clifton (1987) examined the critical conditions for the quasi-static solution to become unbounded at a finite time ($t = t_{\mathrm{cr}}$, say) and related this feature to the onset of localization for this class of problems. The critical time corresponding to the solution unboundness was viewed as the initiation strain for flow localization. Comparisons with experimental observations indicate that such predictions for the initiation strain consistently underestimate the strain needed for the onset of flow localization. In this section, we examine the validity of the quasi-static approximation as well as the connection between the onset of localization and the failure of the quasi-static approximation. For this purpose we combine expressions (14) and (9) to calculate the local inertia term associated with the quasi-static solution

$$\bar{I}(x, t) \equiv \rho \frac{\partial \bar{v}(x, t)}{\partial t} = \rho \left\{ \frac{\mathrm{d}^2 \bar{\gamma}}{\mathrm{d}t^2} + \frac{\ddot{\mathscr{G}}(t)}{\mu} \right\} (x - \tfrac{1}{2}). \tag{15}$$

In eqn (15), the homogeneous plastic strain, $\bar{\gamma}(t)$, is obtained by solving the non-linear system of ordinary differential equations (13). Examination of eqn (15) indicates that the inertia term $\bar{I}(x, t)$ does not vanish in general. Moreover, the maximum absolute value of the above inertia term, denoted by $\bar{I}_{\mathrm{m}}$, occurs at the slab boundaries and is given by

$$\bar{I}_{\mathrm{m}}(t) = \frac{\rho}{2} \left| \frac{\mathrm{d}^2 \bar{\gamma}}{\mathrm{d}t^2} + \frac{\ddot{\mathscr{G}}(t)}{\mu} \right| = \frac{\rho}{2} |\dot{\alpha}(t)|. \tag{16}$$

In view of the above expressions, it is interesting to observe that the unboundness of the quasi-static solution (which implies that $\mathrm{d}\bar{\phi}/\mathrm{d}t \to \infty$) is associated with the unboundness of the inertia term (16). This indicates that flow localization, in this framework, is tied to the mathematical failure of the quasi-static approximation. An alternative approach for examining the role of inertia as regards shear band formation is based on evaluating the rate of change of the total kinetic energy of the system

$$\dot{K}(t) \equiv \frac{\mathrm{d}}{\mathrm{d}t}\left\{\int_0^1 \frac{\rho v^2(\zeta,t)}{2}\mathrm{d}\zeta\right\} = \int_0^1 v\frac{\partial \tau}{\partial x}\mathrm{d}x. \tag{17}$$

A rigorous homogeneous solution must satisfy: $\dot{K}(t) = 0$, $t \geqslant 0$.† However, there is a non-zero value of the kinetic energy associated with the approximate quasi-static solution. Here, we calculate the rate of change of the total kinetic energy associated with the quasi-static solution and relate its growth (i.e. the deterioration of the quasi-static approximation) to the onset of shear localization. Making use of the quasi-static solution together with expression (17), we obtain

$$\dot{\bar{K}}(t) = \frac{\operatorname{sgn}\{\dot{\alpha}(t)\}}{6}\left[\bar{\phi}(t) + \frac{\dot{\mathscr{G}}(t)}{\mu}\right]\bar{I}_{\mathrm{m}}(t) = \frac{\rho}{24}\frac{\mathrm{d}}{\mathrm{d}t}[\alpha(t)]^2. \tag{18a}$$

The above expression indicates that the rate of change of the total kinetic energy becomes unbounded as soon as $t \to t_{\mathrm{cr}}$. Further, it is useful to express the above measures of inertial effects in terms of the localization damage parameter D_{sb} introduced by Shawki and Clifton (1989):‡

$$\dot{\bar{K}}(t) = \frac{\rho}{12}\frac{\dot{D}_{\mathrm{sb}}(t)}{[1-D_{\mathrm{sb}}(t)]^3} = \frac{1}{6}\frac{\operatorname{sgn}\{\dot{\alpha}(t)\}}{1-D_{\mathrm{sb}}}\bar{I}_{\mathrm{m}}(t). \tag{18b}$$

Severe localization was related by Shawki and Clifton (1989) to the critical time t_{cr}: $D_{\mathrm{sb}}(t_{\mathrm{cr}}) = 1$. Examination of expressions (18) indicates that both measures of inertial effects become unbounded as soon as $D_{\mathrm{sb}} \to 1$. Moreover, we observe that§

$$\frac{\bar{I}_{\mathrm{m}}(t)}{\bar{\phi}(t)} = \frac{\rho}{2}\frac{|\dot{D}_{\mathrm{sb}}(t)|}{1-D_{\mathrm{sb}}(t)} = 6[1-D_{\mathrm{sb}}(t)]\operatorname{sgn}\{\dot{\alpha}(t)\}\frac{\dot{\bar{K}}(t)}{\bar{\phi}(t)}. \tag{19}$$

In view of the boundness of $\dot{D}_{\mathrm{sb}}(t_{\mathrm{cr}})$, the above expressions imply that the quotients $\bar{I}_{\mathrm{m}}/\bar{\phi}$ and $\dot{\bar{K}}/\bar{\phi}$ are singular in the neighborhood of the critical time t_{cr}. The singularities are of orders "-1" and "-2", respectively. In other words, the maximum inertia and the rate of change of total kinetic energy become unbounded at faster rates as compared with the rate of growth of the plastic strain rate, i.e. the approximate, homogeneous quasi-static solution breaks down before the critical time t_{cr} is reached.

For illustration purposes, we consider the class of thermal-viscoplastic solids modeled by the empirical power law,

$$\tau = \theta^{\nu}(\gamma/\gamma_0)^n\dot{\gamma}^m \quad \text{or} \quad \dot{\gamma} = \theta^{p}(\gamma/\gamma_0)^q\tau^r, \tag{20a}$$

†This must be true because of the vanishing of the stress gradient for a homogeneous solution.

‡Following Shawki and Clifton (1989), the local exact solution for the plastic strain rate of the non-linear system (1) corresponding to the deformation conditions considered in the current work (with no elastic effects and constant stress boundary conditions) is given by

$$\frac{\phi(t)}{\phi(0)} = \frac{1}{1-D_{\mathrm{sb}}(t)}, \quad D_{\mathrm{sb}} \equiv -\phi(0)\int_0^1 \frac{C_{\mathrm{p}}(\eta)}{S_{\dagger}^{*}(\eta)}\mathrm{d}\eta.$$

In the above expressions, C_{p} stands for the slope of the adiabatic stress–strain curve at constant strain rate whereas $S_{\dagger}^{*}$ is a logarithmic measure of strain rate sensitivity. These quantities are given by

$$C_{\mathrm{p}} \equiv S_3 + r_1\tau S_2, \quad S_{\dagger}^{*} \equiv \partial f/\partial \ln \phi.$$

§Note that this comparison holds only for rigid material response, adiabatic deformations and constant stress boundary conditions for which $\mathscr{G}(t) = \mathscr{G}_0 \Rightarrow \alpha(t) = 1/(1-D_{\mathrm{sb}}(t)) = \dot{\phi}(t)$; $\phi(0) = 1$.

where

$$p \equiv -v/m, \quad q \equiv -n/m, \quad r \equiv 1/m, \tag{20b}$$

where all exponents assume constant, material-dependent values. Furthermore, we consider the prescribed boundary stress to be prescribed by

$$\mathscr{S}(t) = \left\{ \begin{array}{cc} 0 & t < -t_1 \\ 1+(t/t_1) & -t_1 \leqslant t < 0 \\ 1 & t \geqslant 0 \end{array} \right\}, \tag{21}$$

for some positive constant t_1. The homogeneous quasi-static solution is simply given by

$$\int_1^{\bar{\Gamma}(t)} [1+r_1\gamma_0(\eta-1)]^{-p}\eta^{-q}\,\mathrm{d}\eta = \frac{t}{\gamma_0}; \quad \bar{\Gamma}(t) \equiv \frac{\bar{\gamma}(t)}{\gamma_0} \tag{22a}$$

$$\bar{\theta}(t) = 1+r_1\gamma_0[\bar{\Gamma}(t)-1] \tag{22b}$$

$$\bar{\phi}(t) = \gamma_0 \frac{\mathrm{d}\bar{\Gamma}(t)}{\mathrm{d}t}. \tag{22c}$$

Molinari and Clifton (1983) first noted that a necessary condition for the unboundness of the solution of the quadrature in eqn (22a) at a finite critical time, $t = t_{cr}$ (say), is given by

$$p+q > 1 \quad \text{or} \quad v+n+m < 0. \tag{23}$$

The above condition was viewed by Molinari and Clifton (1983) and, Molinari and Clifton (1987) as a necessary condition for the onset of localization in power law materials. The critical time t_{cr} for the onset of localization is provided by

$$t_{cr} = \gamma_0 \int_1^{\infty} [1+r_1\gamma_0(\eta-1)]^{-p}\eta^{-q}\,\mathrm{d}\eta, \quad p+q > 1. \tag{24}$$

In the special case where $n = 0$ ($q = 0$) the power law material model (20) may be viewed as describing the behavior of a non-Newtonian fluid with temperature-dependent viscosity. Subject to such conditions, the solution (22) can be evaluated explicitly to obtain

$$\bar{\phi}(t) = \{1+r_1(1-p)t\}^{\frac{p}{1-p}} = \bar{\theta}(t)^p \quad \text{for} \quad p \neq 1, \tag{25a}$$

while

$$\bar{\phi}(t) = \bar{\theta}(t) = \exp\{r_1 t\} \quad \text{for} \quad p = 1. \tag{25b}$$

Next, we use the quasi-static solution (25) to examine the evolution of the following normalized quantities:

$$E_1(t) \equiv \frac{\bar{\phi}(t)}{\bar{\phi}(0)} = \{1+r_1(1-p)t\}^{\frac{p}{1-p}} = \left\{1-\frac{t}{t_{cr}}\right\}^{\frac{p}{1-p}} \tag{26a}$$

$$E_2(t) \equiv \frac{\bar{I}_m(t)}{\bar{I}_m(0)} = \{1+r_1(1-p)t\}^{\frac{2p-1}{1-p}} = \left\{1-\frac{t}{t_{cr}}\right\}^{\frac{2p-1}{1-p}} \tag{26b}$$

$$E_3(t) \equiv \frac{\bar{\dot{K}}(t)}{\bar{\dot{K}}(0)} = \{1+r_1(1-p)t\}^{\frac{3p-1}{1-p}} = \left\{1-\frac{t}{t_{cr}}\right\}^{\frac{3p-1}{1-p}}, \tag{26c}$$

where

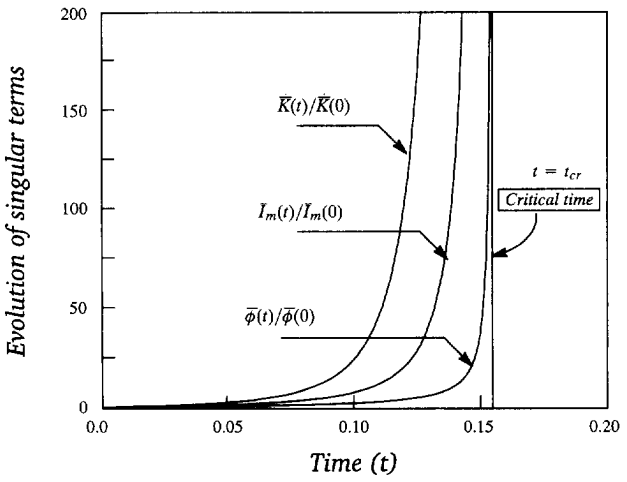

Fig. 3. Evolution of the singular terms given by eqns (26a–d).

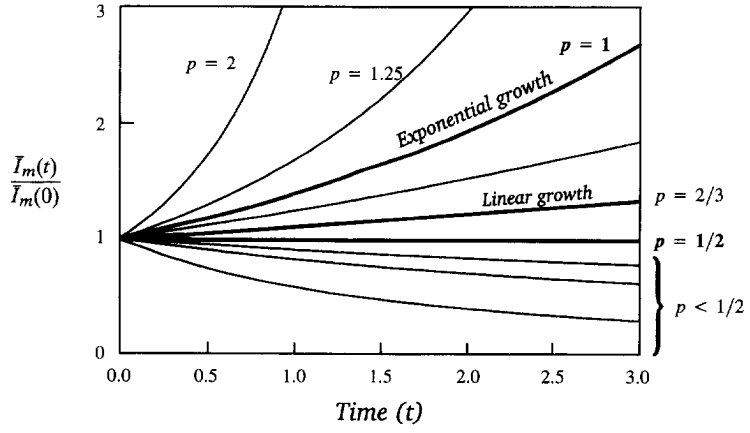

Fig. 4. Evolution of inertial effects during the quasi-static deformation of a non-Newtonian fluid with temperature-dependent viscosity.

$$t_{cr} = \frac{-1}{r_1(1-p)}, \quad p > 1. \tag{26d}$$

Figure 3 illustrates the behavior of the functions in eqns (26a–d) for the case where $p = 20$ and $r_1 = 0.34$ which are representative values of a typical structural steel. Examination of Fig. 3 indicates that, as t approaches the critical value t_{cr}, the quasi-static approximation breaks down. It is important to observe that the breakdown of the quasi-static approximation, measured by larger values of either $E_2(t)$ or $E_3(t)$, takes place at much earlier times than the "critical time". The failure of the quasi-static approximation implies that an *inhomogeneous* flow field emanates from the originally near-homogeneous, quasi-static field which gives rise to shear localization in the sense of shear strain concentration within narrow boundary layers (where inertial effects are most significant). This very connection between the onset of shear localization (severe deformation inhomogeneity) and the increased importance of inertial effects is the primary focus of this work.

Figure 4 illustrates the dependence of the evolutionary behavior of $\bar{I}_m(t)/\bar{I}_m(0)$ on the material response through considering different values of the exponent p. Note that the inertia associated with the quasi-static solution grows exponentially with time for materials with $p > 1$. In fact, for materials with $2p > 1$, the inertia term grows monotonically with time and the homogeneous quasi-static solution eventually breaks down, albeit at a much slower rate than that corresponding to materials with $p > 1$. Next, we seek to explore the

structure of the inhomogeneous field that takes place as soon as inertial (dynamic) effects become significant.

5. ANALYSIS OF A MODEL PROBLEM

In order to examine the influence of inertia on the evolution of inhomogeneous deformation as well as its localization retardation effect, we neglect elastic effects, by setting $\mu = \infty$ in eqn (1b), and eliminate the velocity from eqns (1a,b) while taking advantage of the energy equation (1c) to obtain

$$\frac{\partial \tau}{\partial t} = \left\{\frac{S_1(x,t)}{\rho}\right\}\frac{\partial^2 \tau}{\partial x^2} + C_p(x,t)\phi(x,t). \tag{27a}$$

The above non-linear partial differential equation should be satisfied by any smooth (classical) solution of the initial boundary-value problem, described by eqns (1a–e) as well as the auxiliary conditions (6) and (7). Conversely, if we know the solution to the posed initial boundary-value problem except for the flow stress $\tau(x,t)$, then we must be able to solve eqn (27a) together with the auxiliary conditions

$$\tau(x,0) = 1, \quad \tau(0,t) = \tau(1,t) = \mathscr{G}(t) \quad \text{for} \quad t > 0 \tag{27b}$$

for the correct flow stress $\tau(x,t)$. It is evident that the non-linearity of eqns (1a–e) presents a serious difficulty as regards finding exact analytic solutions. Therefore, we introduce a model problem that is sought to retain the basic mathematical structure of eqn (27a) while admitting a closed-form solution. For this purpose, we suggest the following initial boundary-value problem:

$$\frac{\partial \tau}{\partial t} = \delta^2 \frac{\partial^2 \tau}{\partial x^2} + B_0, \tag{28a}$$

with

$$\tau(x,0) = \tau(0,t) = \tau(1,t) = 1. \tag{28b}$$

In writing eqn (28a), we have used the boundary stress prescription given by eqn (21). Furthermore, the term δ^2 in eqn (27a) is a constant that replaces the quotient $S_1(x,t)/\rho$. Although B_0 replaces a term that depends on both space and time, the approximation introduced is expected to have a secondary effect as regards the spatial structure for the flow stress. It is important to note that the *sign* of the term B_0 parallels that of the slope of the adiabatic stress–strain rate at a constant strain rate, i.e. $C_p(x,t)$.

5.1. *Exact solution*

The complete solution of the linear model problem (28) can be obtained through a variety of standard techniques and is given by

$$\tau(x,t) = 1 + \left\{\left(\frac{4B_0}{\delta^2}\right)\sum_{n=1}^{n=\infty} u_n(x,t)\right\}, \tag{29a}$$

where

$$u_n(x,t) = \frac{\sin(\xi_n x)}{\xi_n^3}\{1 - \exp[-\delta^2 \xi_n^2 t]\}, \quad \xi_n \equiv (2n-1)\pi. \tag{29b}$$

A number of useful observations can now be made. First, we note that the term enclosed

by braces in eqn (29a) represents inertial effects since it vanishes in the quasi-static limit $\rho \to 0$. More specifically, as $\rho \to 0$ then $\delta^2 \to \infty$ and $\tau(x, t) \to 1$ which corresponds to the quasi-static solution for the problem posed. Therefore, the solution (29) may be viewed as the superposition of the approximate quasi-static solution and an "inertial correction term". Furthermore, the behavior of the solution (29) depends on inertia and material rate sensitivity through the quotient $S_1(x, t)/\rho \leftrightarrow \delta^2$. This suggests that the quotient $S_1(x, t)/\rho$ is the channel through which the interactive roles of inertia and rate sensitivity are displayed and it is, therefore, expected to play a primary role as regards the qualitative behavior of solutions. Further examination of the solution (29) implies that the inertial correction term is dominated by the large wavelength components of the series solution (i.e. smaller values of ξ_n for fixed values of other parameters). Further, we explore the structure of the solution (29) in the two limiting cases corresponding to very small and very large values of δ^2:

5.1.1. *Inertial stresses* $\gg$ *viscous stresses* ($\delta^2 \to 0$). In this case, the solution (29) reduces to

$$u_n(x, t) = \frac{\sin(\xi_n x)}{\xi_n}[(\delta^2 t) + (\delta^2 \xi_n t)^2 + O(\delta^2)^3] \tag{30a}$$

$$\tau(x, t) = 1 + (4B_0)\sum_{n=1}^{n=\infty} \sin(\xi_n x)\left[\frac{t}{\xi_n} + O(\delta^2)\right]. \tag{30b}$$

Evaluation of the summation in eqn (30b) provides the simpler solution form†

$$\tau(x, t) = 1 + B_0 t, \quad \text{as} \quad \delta^2 \to 0. \tag{31}$$

It is important to note that this solution does *not* satisfy the imposed stress boundary conditions. This is due to the fact that, in this limit as $\delta^2 \to 0$, the partial differential equation (28a) reduces to an ordinary differential equation that is incapable of satisfying the boundary conditions in eqn (28b). However, this solution will be shown to coincide with the outer solution of a singular perturbation version of the considered model problem. That is, the solution (30) is valid for sufficiently small values of δ^2 away from the boundaries.

5.1.2. *Viscous stresses* $\gg$ *inertial stresses* ($\delta^2 \to \infty$). In this case, the solution (29) reduces to

$$\left.\begin{aligned} &u_n(x, t) \to \frac{\sin(\xi_n x)}{\xi_n^3}, \\ \text{hence} \qquad &\tau(x, t) \to 1 + \left(\frac{4B_0}{\delta^2}\right)\sum_{n=1}^{n=\infty} \frac{\sin(\xi_n x)}{\xi_n^3} \to 1, \end{aligned}\right\} \quad \text{as} \quad \delta^2 \to \infty, \tag{32}$$

i.e. the solution (29) to our model problem (28) reduces to the quasi-static solution in the limit where viscous stresses are much larger than inertial stresses. At this point, it is important to observe that it is the relative weight of inertial to viscous stresses which controls the solution.

†It is useful to note that

$$\sum_{n=1}^{n=\infty} \frac{\sin[(2n-1)\pi x]}{(2n-1)\pi} = \tfrac{1}{4} \quad \text{for} \quad x \in [0, 1].$$

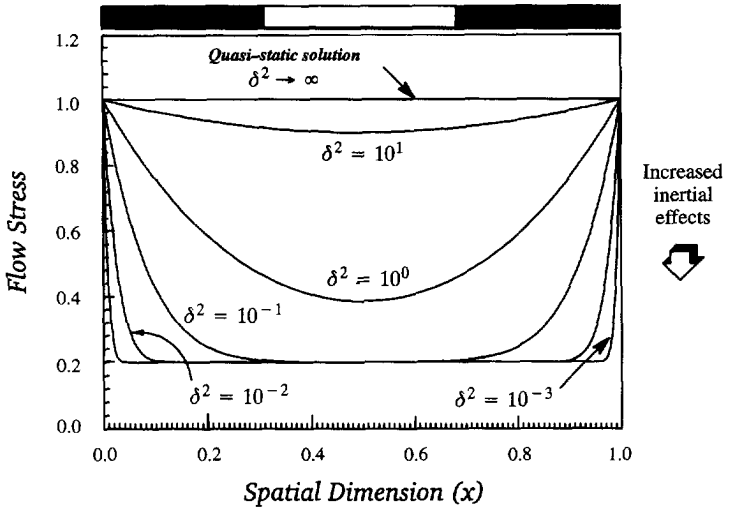

Fig. 5. Exact solution of the model problem (28) for different values of δ^2.

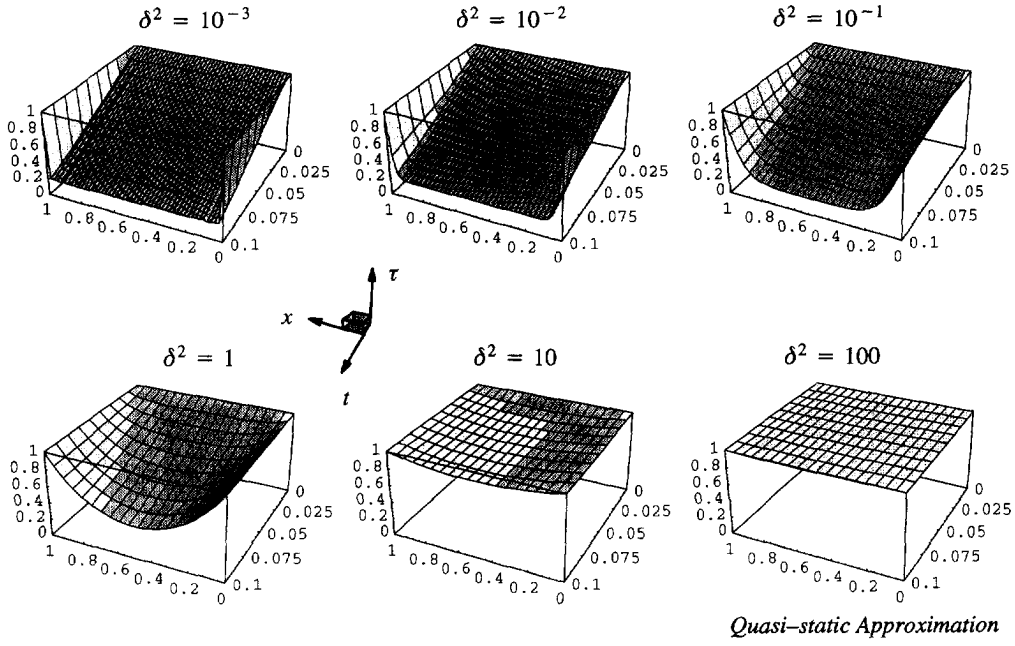

Fig. 6. Behavior of the exact solution (29) for different values of δ^2.

Figure 5 illustrates the behavior of the exact solution (29) for a spectrum of δ^2 values in the range $[10^{-3}, 10^2]$. The profiles shown in Fig. 5 are obtained by calculating a partial sum of the series solution (29) that uses 100 terms. Further, we have used the values $B_0 = -8$, $\Delta x = 0.005$ while evaluating the solution at the time $t = 0.1$.† It is important to note that the solution associated with small values of δ^2 exhibits a boundary layer-like structure in the neighborhood of specimen boundaries. The thickness of this boundary layer decreases with decreasing values of δ^2. This behavior suggests that the model problem (28) is a singular perturbation problem for small values of δ^2. The key to the shaded bar at the top of Fig. 5 will be explained in the next section. Figure 6 provides the evolution of

†The selection of 100 terms for the evaluation of the series solution (29) is based on the convergence characteristics of the series solution. Further, the increment Δx is used for plotting purposes while the selection of $B_0 = -8$ is intended to reflect a situation in which the slope C_p has become sufficiently negative in order to simulate severe localization.

the stress fields, obtained through the exact solution (29), for the same values of δ^2 used in Fig. 5.

The stress behavior illustrated in Fig. 6 indicates that the quasi-static approximation is only appropriate for sufficiently large values of the dimensionless quotient $S_1(x,t)/\rho$. Values greater than 100 are viewed as sufficiently large. Large values of the quotient $S_1(x,t)/\rho$ correspond to either slow rates of loading or strong strain rate sensitivity. Moreover, it should be noted that this quotient depends on both position and time. In fact, the typical behavior of this quotient within a localizing zone is that it decays monotonically. This behavior suggests the insufficiency of the quasi-static approximation for problems involving dynamic flow localization.

6. THE SINGULAR PERTURBATION PROBLEM

In this section, we examine the detailed spatial structure as well as the temporal evolution of solutions to the model problem (28) in the case where inertial stresses dominate viscous stresses. For this purpose, we take advantage of the problem symmetry and consider the following initial boundary-value problem:

$$\frac{\partial \tau}{\partial t} = \varepsilon \frac{\partial^2 \tau}{\partial x^2} + B_0, \quad \varepsilon \ll 1, \quad B_0 = O(1), \tag{33a}$$

with

$$\tau(x,0) = \tau(0,t) = 1 \quad \text{and} \quad \frac{\partial \tau}{\partial x}(0.5,t) = 0. \tag{33b}$$

Next, we follow a standard procedure of perturbation methods and seek an outer solution that is valid away from the boundaries and an inner solution that describes the behavior in the vicinity of the boundaries. The method of "matched asymptotic expansions" is used in this analysis.

6.1. *The outer solution* $[\tau^{(o)}(x,t)]$

We seek an outer solution, valid away from the boundaries, of the form

$$\tau^{(o)}(x,t) = z_0(x,t) + \varepsilon z_1(x,t) + \ldots = \sum_{k=0}^{k=\infty} \varepsilon^k z_k(x,t), \tag{34a}$$

with

$$z_k(x,0) = \delta_{k0} \quad \text{and} \quad \frac{\partial z_k(0.5,t)}{\partial x} = 0, \tag{34b}$$

for all integers $k \geqslant 0$. In eqns (34b), δ_{ij} is the Kronecker delta. Substitution of the solution (34a) in the governing equation (33a) and collecting terms of the same order of the small parameter ε gives the following set of initial boundary-value problems for the functions $z_k(x,t)$, $k \geqslant 0$:

$$\left.\begin{aligned} &\frac{\partial z_0(x,t)}{\partial t} = B_0 \\ z_0(x,0) = 1 \quad &\text{and} \quad \frac{\partial z_0(0.5,t)}{\partial x} = 0 \end{aligned}\right\} \tag{35a}$$

as well as

$$\left.\begin{aligned} &\frac{\partial z_k(x,t)}{\partial t} = \frac{\partial^2 z_{k-1}(x,t)}{\partial x^2} \\ z_k(x,0) = &\frac{\partial z_k(0.5,t)}{\partial x} = 0 \end{aligned}\right\} k \geqslant 1. \tag{35b}$$

It is straightforward to verify that all the initial boundary-value problems given by eqn (35b) have a vanishing solution. Hence, the outer solution coincides with the zeroth-order term in the expansion (34a), i.e.

$$\tau^{(o)}(x,t) = 1 + B_0 t. \tag{36}$$

Furthermore, note that the outer solution (36) is the same as the limit of the exact solution (29a) as $\delta^2 \to 0$, see expression (31) in Section 5.1. This implies that the outer solution expresses the response in the spatial interval far from the boundaries where inertial effects overwhelm viscous effects.

6.2. *The inner solution* $[\tau^{(i)}(x, t)]$

Here, we seek an inner solution that is valid in the vicinity of the boundary $x = 0$. For this purpose, we introduce the magnified space variable ζ defined by

$$\zeta \equiv x/\varepsilon^{\lambda}, \tag{37}$$

where $\lambda > 0$ is a constant to be determined from the analysis. In terms of the new variable ζ, eqns (33a,b) reduce to

$$\frac{\partial \tau^{(i)}(\zeta,t)}{\partial t} = \varepsilon^{1-2\lambda} \frac{\partial^2 \tau^{(i)}(\zeta,t)}{\partial \zeta^2} + B_0, \tag{38a}$$

with

$$\tau^{(i)}(\zeta,0) = \tau^{(i)}(0,t) = 1. \tag{38b}$$

The choice $\lambda = 1/2$ appears to be the most appropriate for the considered problem: see, for example, Nayfeh (1973). We now assume an inner solution of the form

$$\tau^{(i)}(\zeta,t) = \omega_0(\zeta,t) + \varepsilon\omega_1(\zeta,t) + \ldots = \sum_{k=0}^{k=\infty} \varepsilon^k \omega_k(\zeta,t), \tag{39a}$$

with

$$\omega_k(\zeta, 0) = \omega_k(0, t) = \delta_{k0}, \quad \forall k \geqslant 0. \tag{39b}$$

Substitution of eqns (39a,b) in the governing equation (38) gives the following initial boundary-value problems for the functions $\omega_k(\zeta, t)$, $k \geqslant 0$:

$$\left.\begin{aligned} \frac{\partial \omega_0(\zeta, t)}{\partial t} &= \frac{\partial^2 \omega_0(\zeta, t)}{\partial \zeta^2} + B_0 \\ \omega_0(\zeta, 0) &= \omega_0(0, t) = 1 \end{aligned}\right\} \tag{40a}$$

and

$$\left.\begin{aligned} \frac{\partial \omega_k(\zeta, t)}{\partial t} &= \frac{\partial^2 \omega_k(\zeta, t)}{\partial \zeta^2} \\ \omega_k(\zeta, 0) &= \omega_k(0, t) = 0 \end{aligned}\right\} k \geqslant 1. \tag{40b}$$

Complete description of the problem for the inner solution requires the additional condition that

$$\lim_{\zeta \to \infty} \left\{ \frac{\partial \omega_k(\zeta, t)}{\partial \zeta} \right\} = 0, \quad \forall k \geqslant 0, \tag{41}$$

in order to be consistent with the outer solution $\tau^{(o)}(x, t)$. Subject to the foregoing conditions, it is evident that the unique solution to all the problems in eqn (40b) is the zero solution. Hence, the inner solution is completely described by the zeroth-order term in the expansion (39a) which can be determined through solving eqn (40a) together with the consistency (matching) requirement given by eqn (41) to obtain

$$\tau^{(i)}(\zeta, t) = (1 + B_0 t) - (B_0 t)\left[(1 + 2\Omega^2)\,\mathrm{erfc}\,(\Omega) - \frac{2\Omega}{\sqrt{\pi}} \mathrm{e}^{-\Omega^2} \right], \quad \Omega \equiv \frac{\zeta}{2\sqrt{t}}. \tag{42}$$

In eqn (42), the notation erfc(x) denotes the complementary error function of x. Comparison of expressions (42) and (36) allows us to rewrite the inner solution as

$$\tau^{(i)}(\zeta, t) = \tau^{(o)}(x, t) - (B_0 t) H(\Omega(\zeta, t)), \tag{43}$$

where $H(\Omega)$ is the term enclosed by square brackets in expression (42). Examination of expression (43) implies that $H(0) = 1$ so that the solution (43) satisfies the end condition $\tau^{(i)}(0, t) = 1$. Furthermore, it is easy to verify that $H(\infty) = 0$ so that the consistency condition (41) is exactly satisfied. The complete solution to the considered singular perturbation problem (33) may now be summarized as follows:

$$\tau(x, t) = \begin{cases} 1 + B_0 t & \text{for } \delta < x < 0.5 \\ 1 + B_0 t \left\{ 1 - H\left(\dfrac{x}{2\delta\sqrt{t}} \right) \right\} & \text{for } 0 \leqslant x < \delta. \end{cases} \tag{44}$$

It is interesting to note that the inner solution describes the solution of the model problem (32) within a *boundary layer whose thickness is proportional to* δ. For each profile in Fig. 5, with a value of $\delta^2 < 1$, the thickness of this layer is computed based on the asymptotic solution as being simply δ. These analytically-computed thicknesses are shown on the top bar with different levels of shading intensity. Comparison of the computed thicknesses with

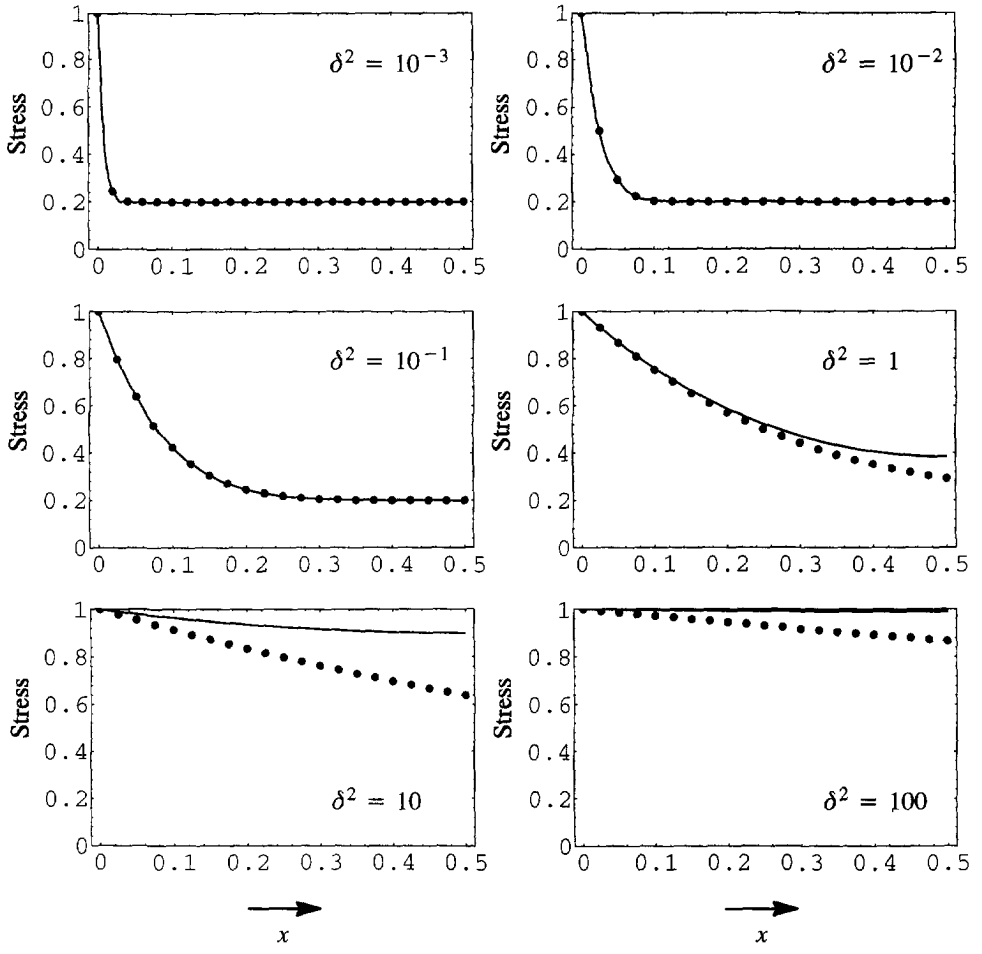

Fig. 7. Comparison of the exact solution (solid lines), given by eqn (29), with the asymptotic solution (solid circles), given by eqn (44).

those obtained from plotting the exact solution (29) shows excellent agreement. Figure 7 examines the validity of the asymptotic solution (44) through a comparison with the exact solution (29) of our model problem. As expected, the two solutions exhibit excellent agreement for values of $\delta < 1$. The asymptotic solution (44) breaks down for higher values of δ.

The spatial structure of the boundary layer for $\delta < 1$ is described entirely by the function

$$H(\Omega) = (1+2\Omega^2)\,\mathrm{erfc}\,(\Omega) - \frac{2\Omega}{\sqrt{\pi}}\mathrm{e}^{-\Omega^2}. \tag{45}$$

We will refer to this function as the shear band shape function. Figure 8 provides a graphical illustration of its behavior.

Here, we recall that δ^2 replaces the ratio S_1/ρ. Moreover, we point out that the sign of the lower-order term B_0 in eqn (33a) determines whether the outer solution grows ($B_0 > 0$) or decays ($B_0 < 0$). This simulates the effect of the sign of the slope C_p of the adiabatic stress–strain curve at a constant strain rate on the behavior of the flow stress for the non-linear problem. It is also useful to observe that the unique solution to the model problem (33) when $B_0 = 0$ is the quasi-static (spatially uniform) solution $\tau(x, t) = 1$. In terms of the graphical representation of Fig. 2, and during a constant strain rate test, the situation associated with $B_0 \leftrightarrow C_p = 0$ corresponds to

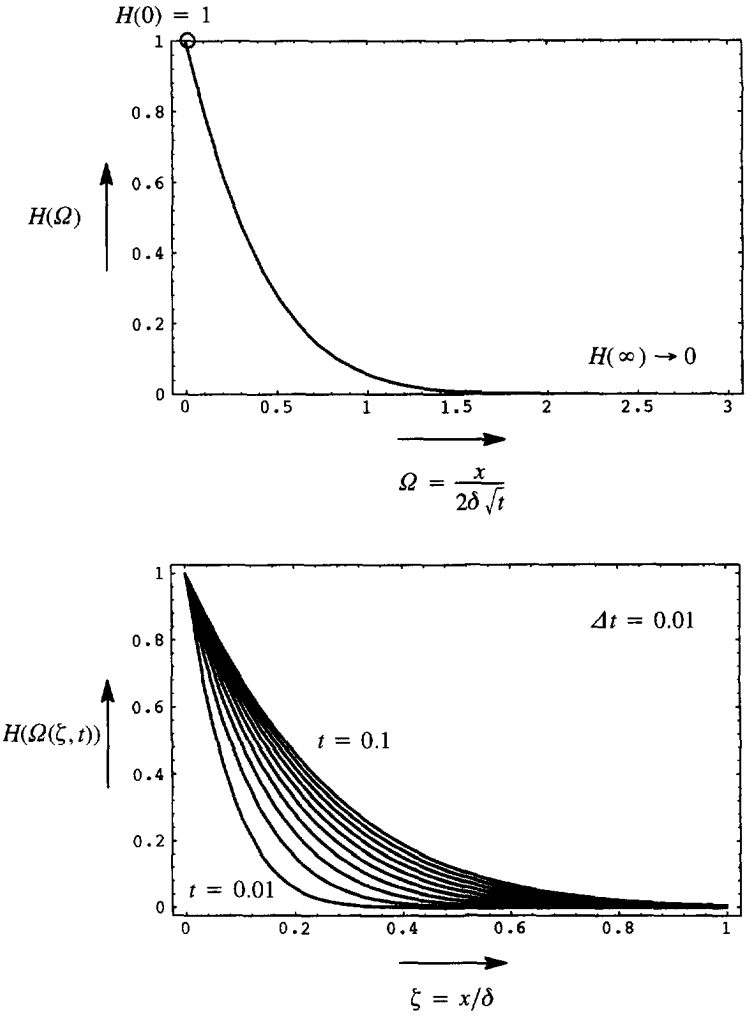

Fig. 8. The shear band shape function $H(\Omega)$.

$$d\tau = \mathbf{S} \cdot d\mathbf{z} = 0, \tag{46}$$

i.e. the evolution of an inhomogeneous deformation field, for our considered problem, is related to the non-orthogonality of the material response vector $\mathbf{S}$ to the vector $d\mathbf{z} = (0, d\theta, d\gamma)^T$. The condition (46) also signals increased inertial (dynamic) effects, i.e. the breakdown of the approximate, homogeneous quasi-static solution.

7. EXACT SOLUTION FOR A KELVIN–VOIGT MATERIAL

In this section, we consider a special case for which an exact closed-form solution can be obtained. This solution will be used to support our earlier discussions and provide some additional insights into the considered problem. For this purpose, consider the case in which:

(i) elastic effects can be neglected (i.e. $\mu = \infty$);
(ii) the deformation is isothermal (i.e. $r_0 = r_1 = S_2 = 0$);
(iii) inertial effects are significant;
(iv) stress boundary conditions (21) are applied; and
(v) the material viscoplastic response is described by a Kelvin–Voigt model

$$\tau = S_1\dot{\gamma} + C_p\gamma, \tag{47}$$

where the coefficients S_1 and C_p are taken to be constants. Using the governing equations (1a,b,e) together with the material description (47) gives the following linear system of partial differential equations for the flow stress and the particle velocity:

$$\frac{\partial \tau}{\partial t} = \delta^2 \frac{\partial^2 \tau}{\partial x^2} + S_3 \frac{\partial v}{\partial x} \tag{48a}$$

$$\frac{\partial v}{\partial t} = \frac{1}{\rho}\frac{\partial \tau}{\partial x}, \tag{48b}$$

where

$$c^2 \equiv \frac{S_3}{\rho} \quad \text{and} \quad \delta^2 \equiv \frac{S_1}{\rho} \geqslant 0. \tag{48c}$$

It is useful to note that if the strain $\gamma(x, t)$ in eqn (47) is interpreted as an elastic strain, then real values of c in eqn (48c) would correspond to the elastic shear wave speed. On the other hand, in our case where the material is rigid while exhibiting linear strain hardening (or softening) and strain rate hardening, real values of c in eqn (48c) are interpreted as corresponding to the plastic wave speed. Further, non-vanishing values of δ^2 introduce a diffusion-like behavior to solutions of the governing equation (48a). Next, we introduce the notation

$$G \equiv \frac{C_p}{S_1} = \frac{c^2}{\delta^2}, \tag{49}$$

which represents the ratio of the slope of the adiabatic stress–strain curve at constant strain rate to the material strain rate sensitivity. The auxiliary conditions associated with eqns (48a–c) are given by

$$\tau(0, t) = \tau(1, t) = \tau(x, 0) = 1, \quad \gamma(x, 0) = \gamma_0 \tag{50a}$$

$$\dot{\gamma}(x, 0) = \frac{1 - C_p\gamma_0}{S_1} \equiv \phi_0, \quad v(0.5, t) = \frac{\phi_0}{2}, \quad v(x, 0) = \phi_0 x. \tag{50b}$$

The exact solution of the initial boundary-value problem described by eqns (48a–c) can be obtained if we seek solutions of the form

$$\tau(x, t) = 1 + A(t)\sin\xi_n x, \quad v(x, t) = \frac{\phi_0}{2} + B(t)\cos\xi_n x, \tag{51a}$$

with

$$\xi_n = (2n-1)\pi, \quad n = 1, 2, 3, \ldots \tag{51b}$$

The above solution form satisfies all the auxiliary conditions for the flow stress as well as the center-line condition for the velocity. Substitution in the system (48) provides the exact solution

$$\tau(x,t) = 1+4\phi_0 S_3 \sum_{n=1}^{\infty} d_\tau(\xi_n,t)\frac{\sin\xi_n x}{\xi_n} \tag{52a}$$

and

$$v(x,t) = \frac{\phi_0}{2}+4\phi_0 \sum_{n=1}^{\infty} d_v(\xi_n,t)\frac{\cos\xi_n x}{\xi_n^2}, \tag{52b}$$

where

$$d_\tau(\xi_n,t) = \frac{e^{P_n^+ t}-e^{P_n^- t}}{P_n^+-P_n^-}, \quad d_v(\xi_n,t) = \frac{P_n^+ e^{P_n^- t}-P_n^- e^{P_n^+ t}}{P_n^+-P_n^-} \tag{53a}$$

and

$$P_n^{\pm} = \tfrac{1}{2}[-a_1 \pm \sqrt{(a_1^2-4a_0)}], \quad a_1 = (\xi_n\delta)^2, \quad a_0 = (\xi_n c)^2 = Ga_1. \tag{53b}$$

The solutions for the plastic strain and plastic strain rate are obtained by substituting expression (52a) in the material description equation (47) and hence integrating the resulting equation to obtain

$$\gamma(x,t) = \gamma_0 e^{-Gt}+(1-e^{-Gt})/C_p+4\phi_0 S_3 \sum_{n=1}^{\infty} d_\gamma(\xi_n,t)\frac{\sin\xi_n x}{\xi_n} \tag{54a}$$

$$\dot\gamma(x,t)/\phi_0 = e^{-Gt}+4G \sum_{n=1}^{\infty} d_\gamma(\xi_n,t)\frac{\sin\xi_n x}{\xi_n}, \tag{54b}$$

where

$$d_\gamma(\xi_n,t) = \frac{(e^{P_n^+ t}-e^{-Gt})/(P_n^++G)-(e^{P_n^- t}-e^{-Gt})/(P_n^-+G)}{P_n^+-P_n^-}. \tag{54c}$$

The qualitative behavior of the above solution in the two important cases corresponding to (i) $\delta^2 \to 0$ and (ii) $\delta^2 \to \infty$ is illustrated in Table 3. In the limit (i), the solution behavior

Table 3. Qualitative behavior of the exact solution (52)

$\delta^2 \to 0$ Rate-independent limit		$\delta^2 \to \infty$ Quasi-static limit
Inertial stresses $\gg$ viscous stresses		Viscous stresses $\gg$ inertial stresses
$P_n^{\pm} \to \pm\xi_n\sqrt{-\frac{C_p}{\rho}}$		$P_n^+ \to 0, \quad P_n^- \to -(\xi_n\delta)^2 \to -\infty$
Define: $p_n \equiv \xi_n\sqrt{(\lvert C_p\rvert/\rho)}$		
$C_p > 0$: Hardening	$C_p < 0$: Softening	
$d_\tau(\xi_n,t) \to [\sin(p_n t)]/p_n$,	$d_\tau(\xi_n,t) \to [\sinh(p_n t)]/p_n$,	$d_\tau(\xi_n,t) \to 0$,
$d_v(\xi_n,t) \to \cos(p_n t)$,	$d_v(\xi_n,t) \to \cosh(p_n t)$,	$d_{v(\xi_n,t)} \to 1$,
$d_\gamma(\xi_n,t) \to$	$d_\gamma(\xi_n,t) \to$	$d_\gamma(\xi_n,t) \to 0$,
$\frac{[G\sin(p_n t)]/(p_n)+[e^{-Gt}-\cos(p_n t)]}{G^2+p_n^2}$	$\frac{[G\sinh(p_n t)]/(p_n)+[e^{-Gt}-\cosh(p_n t)]}{G^2-p_n^2}$	
Diffusionless plastic wave propagation	The exact solution *diverges*! This is often called "wave trapping" or simply "loss of hyperbolicity"	$\tau(x,t) \to 1$, $v(x,t) \to \phi_0 x$, $\dot\gamma(x,t) \to \phi_0 e^{-Gt}$, $\gamma(x,t) \to \gamma_0 e^{-Gt}+(1-e^{-Gt})/C_p$.

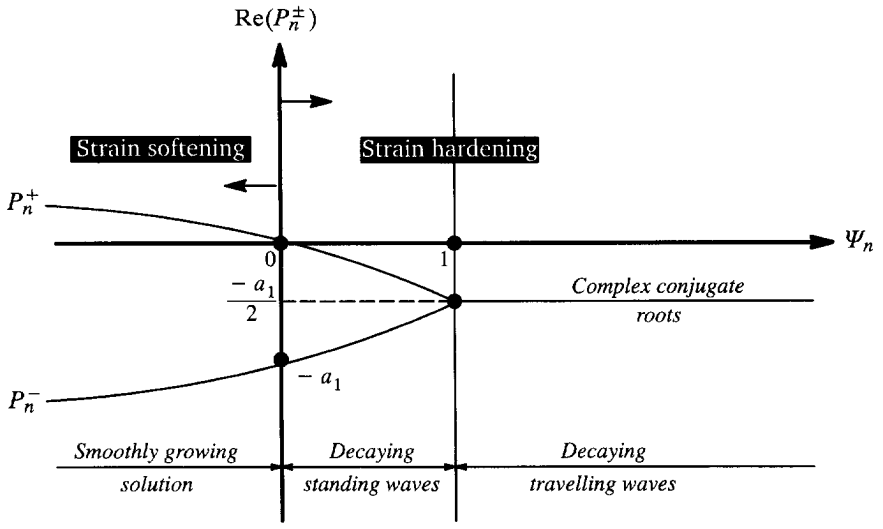

Fig. 9. Behavior of the roots $P_n^{\pm}$ for $\delta^2 \neq 0$.

depends on the sign of $C_p = S_3$. In the case of strain hardening ($C_p > 0$), the solution (52a) describes plastic stress wave propagation whereas in the case of strain softening ($C_p < 0$), the series solution (52a) diverges implying an ill-posed mathematical setup. In fact, if the slope C_p was taken to be a variable that changes sign from positive to negative, then the instant at which it vanishes corresponds to the event called wave trapping by Wu and Freund (1984). This instant is associated with the loss of hyperbolic character for the system (48) which also means that boundary data can no longer be communicated to the interior. On the other hand, in the limit (ii), the solution reduces to the approximate quasi-static solution. Further, we note that in the limit (ii), $d_j(\xi_n, t) \to 0$ and the homogeneous, quasi-static solution for the plastic strain and plastic strain rate may, therefore, be easily deduced from eqns (54a–c).

Without loss of generality, we take $\gamma_0 = 0$ and observe that the solutions (52a) and (54a), at a fixed pair (x, t), depend only on the two parameters G and δ^2; this implies, under the cited conditions, deformations for which G and δ^2 exhibit identical localization responses.

In the foregoing discussion, the limit $\delta^2 \to 0$ may be viewed as corresponding to the rate-independent approximation while the deformation is still regarded as being dynamic. On the other hand, the limit $\delta^2 \to \infty$ may be viewed as corresponding to the quasi-static approximation while the material is still regarded as being rate-dependent. Next, we examine the effect of a non-vanishing δ^2 on the regularization of the ill-posed problem associated with the rate-independent approximation with a softening material response.

Figure 9 illustrates the behavior of the two roots $p_n^{\pm}$ for non-vanishing values of δ^2. It is useful to rewrite these roots as follows:

$$P_n^{\pm} = \frac{-a_1}{2}\{1 \mp \sqrt{(1-\Psi_n)}\}, \quad \Psi_n \equiv \frac{4G}{\xi_n^2 \delta^2} = \frac{4G}{a_1}. \tag{55}$$

In the case of a *strain hardening response* ($G > 0$), we distinguish the two cases (i) $\Psi_n > 1$ and (ii) $\Psi_n \leqslant 1$. In case (i), there exists a critical wavelength $l^* = \delta/(2\sqrt{G})$ above which the components of the series solutions (52) and (54) describe travelling waves with decaying amplitudes and below which the components of the series solutions describe standing waves with decaying amplitudes. On the other hand, in case (ii), all components of the series solutions describe standing waves with decaying amplitudes and no critical wavelength exists.

In the case of a *strain softening response* ($G < 0$), the root P_n^+ is always real and positive whereas the root P_n^- is always real and negative. Careful examination of the series

Table 4. Details of the study cases illustrated in Fig. 7.

Variable	Run a	Run b	Run c	Run d	Run e
C_p	−0.25	−0.1	−0.5	−0.25	0.05
S_1	0.025	0.025	0.125	0.025	0.05
ρ	2.5	2.5	12.5	0.25	0.25
δ^2	0.01	0.01	0.01	0.1	0.2
$G = C_p/\rho$	−0.25	−4	−4	−10	1

solutions (52) and (54) indicates that they are uniformly and absolutely convergent for $\delta^2 \neq 0$. Notice that these series solutions *diverge* when $\delta^2 = 0$. In other words, the mutual presence of inertia and rate dependence retains the well-posedness of the considered problem in the case of a strain softening material response. The absence of one or both of these effects gives rise to a problem that experiences mathematical difficulties as soon as the material exhibits a softening response (refer to Table 1).

Figure 10 illustrates the behavior of the normalized strain rate corresponding to the cases listed in Table 4.

The calculations illustrated in Fig. 10 are obtained by evaluating a partial sum of the series solution (54b) using 100 terms. Furthermore, 100 spatial divisions are used and the profiles correspond to uniform temporal intervals equal to $\Delta t = 0.05$ with the last profile corresponding to a final time $t = 0.2$. Moreover, these results are obtained for $\gamma_0 = 0$. It is useful to note that the results are identical for runs b and c, which confirms our earlier observation regarding the invariance of the response with respect to equal values of the dimensionless numbers G and δ^2. Moreover, it is evident that for small values of δ^2 the solution structure in the vicinity of the boundaries is completely determined by the same two numbers G and δ^2. The maximum value of the normalized plastic strain rate, in the case of strain softening, occurs at the boundaries and is given by

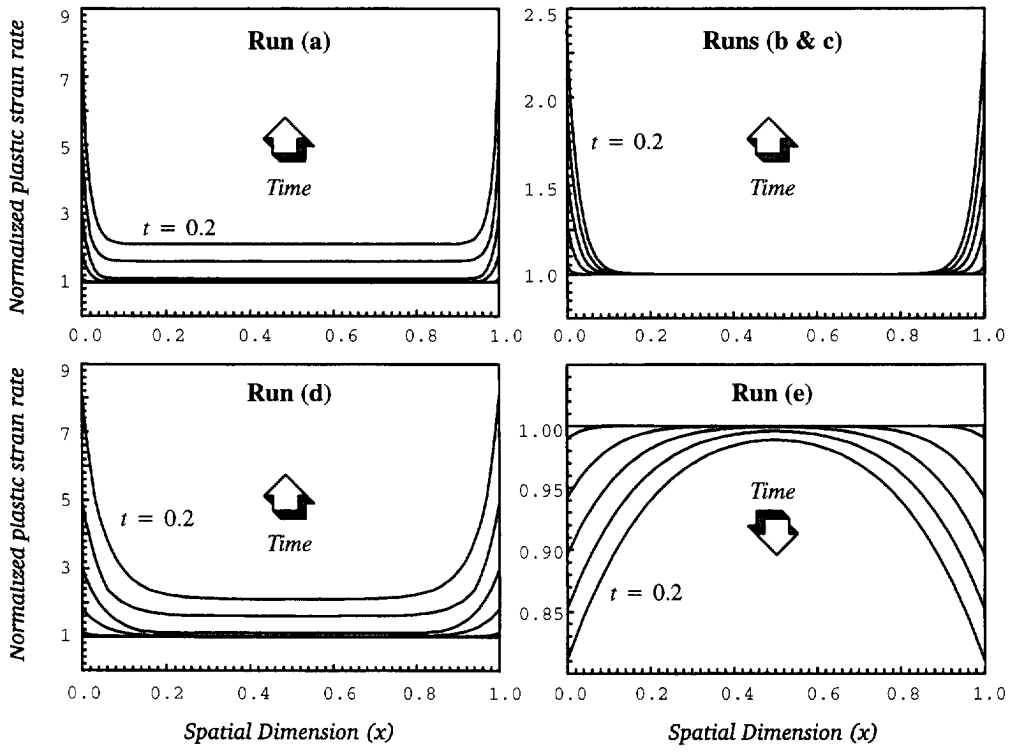

Fig. 10. Exact solution for a Kelvin–Voigt material [normalized strain rate is defined as $\dot{\gamma}(x, t)/\dot{\gamma}(x, 0)$].

$$\dot{\gamma}(0, t)/\dot{\gamma}(0, 0) = \exp\{-Gt\}. \tag{56}$$

Furthermore, the width of the boundary layer in which plastic flow localizes is proportional to δ. A final observation pertains to Fig. 10(e) in which the material exhibits strain hardening and the strain rate decreases in the vicinity of the boundaries.

8. NON-LINEAR NUMERICAL SOLUTIONS

We present a detailed finite difference solution to the initial boundary-value problem described by the governing equations (1a–e) along with auxiliary conditions given by eqns (6) and (7). The purpose of the fully non-linear solution is to verify the validity of conclusions based on the model problem presented in Sections 5 and 6.

8.1. *The finite difference scheme*

The numerical scheme is based on a uniformly divided spatial domain $x \in [0, 0.5]$. Difference equations are based on eqn (27a) together with eqns (1a,b,c) and the second form of eqn (1d). The difference equations for interior nodes are given by

$$D^-(k)\tau_j^n = \left(\frac{S_1}{\rho}\right)_j^n D^+(h)D^-(h)\tau_j^n + (C_p)_j^n D^0(h)v_j^n + (r_0 S_2)_j^n D^+(h)D^-(h)\theta_j^n \tag{57a}$$

$$D^+(k)v_j^n = \frac{1}{\rho} D^0(h)\tau_j^{n+1} \tag{57b}$$

$$(\dot{\gamma}^p)_j^{n+1} = D^0(h)v_j^{n+1} \tag{57c}$$

$$D^+(k)\theta_j^n = r_0 D^+(h)D^-(h)\theta_j^n + r_1(\dot{\gamma}^p)_j^{n+1}\tau_j^{n+1}. \tag{57d}$$

The difference operators used in eqns (57a–d) are defined by

$$D^+(h)u_j^n = (u_{j+1}^n - u_j^n)/h, \quad D^-(h)u_j^n = (u_j^n - u_{j-1}^n)/h \tag{58a}$$

$$D^0(h) = (D^+(h) + D^-(h))/2, \quad D^+(k_n)u_j^n = (u_j^{n+1} - u_j^n)/k_n \tag{58b}$$

$$u_j^n \equiv u(x_j, t_n) = u\left(jh, \sum_{i=1}^{i=n} k_i\right), \quad h \equiv \Delta x, \quad k_n = \sum_{i=1}^{i=n} (\Delta t)_i. \tag{58c}$$

Boundary values for various quantities are obtained through appropriate one-sided difference approximations of the boundary conditions. The variable time step k_n is selected based on the necessary von Neumann stability requirements

$$k_n \leqslant \min_j \left\{\frac{1}{|G_j^n|}, \frac{h^2}{2(\delta^2)_j^n}\right\}. \tag{59}$$

It is useful to note that the two groups δ^2 and G control the stability of the finite difference scheme. These two groups were shown earlier to control the localization response in the case of the model problem (Sections 5 and 6) and the case of a Kelvin–Voigt material (Section 7).

8.2. *Numerical experiments*

This section examines the computed solutions for five test cases labeled as runs 1–5. We used the power law given by eqn (20) to model the material response for all test cases.

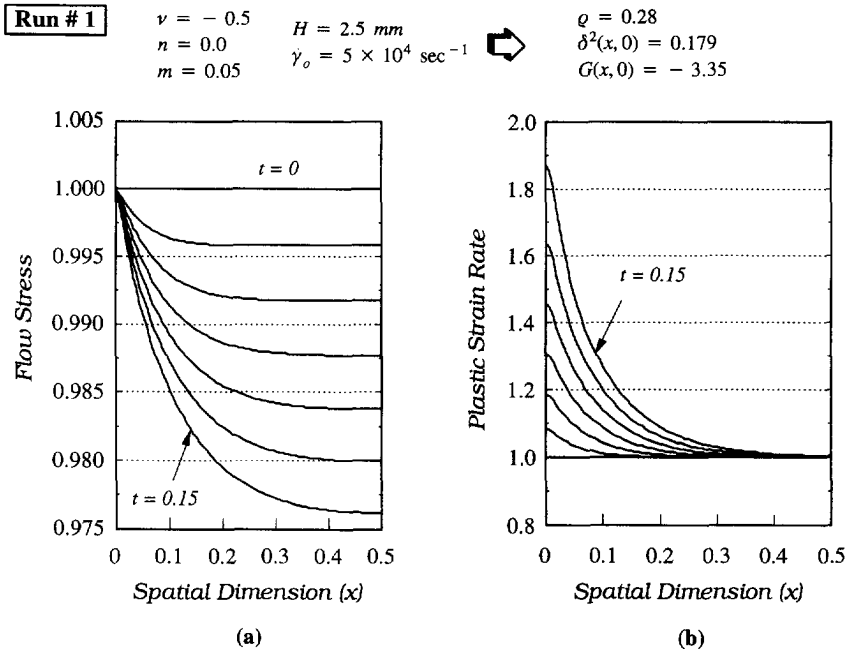

Fig. 11. Spatial evolution of the flow stress and plastic strain rate for run 1.

The spatial domain [0,0.5] is divided into 80 equal numerical elements. Figures 11–14 illustrate the spatial evolution for the flow stress and plastic strain rate for runs 1–4. All five test runs share the following numerical values for various quantities: $\theta_0 = 300°C$, $\tau_0 = 436$ MPa, $\rho = 7800$ kg m^{-3}, $C = 3.9 \times 10^6$ J m^{-3} °C^{-1}, $\beta = 0.9$ and $\gamma_0 = 0.01$. Other quantities are given within each individual figure.

Based on the computed solutions, we can make a number of observations:

(1) Although runs 1 and 2 share the same loading rate, slab dimension and yield strength (and hence the same dimensionless density), their contrasting localization response

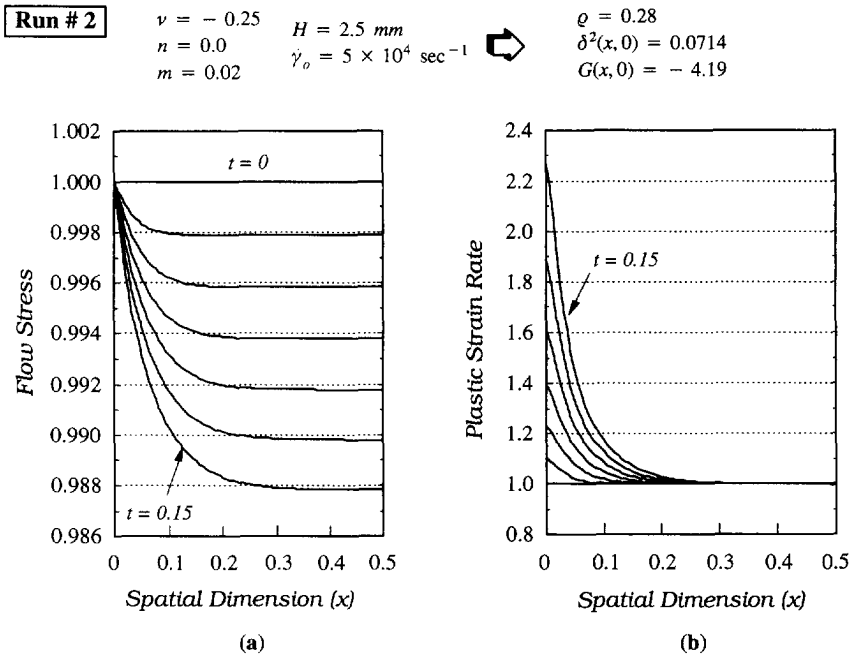

Fig. 12. Spatial evolution of the flow stress and plastic strain rate for run 2.

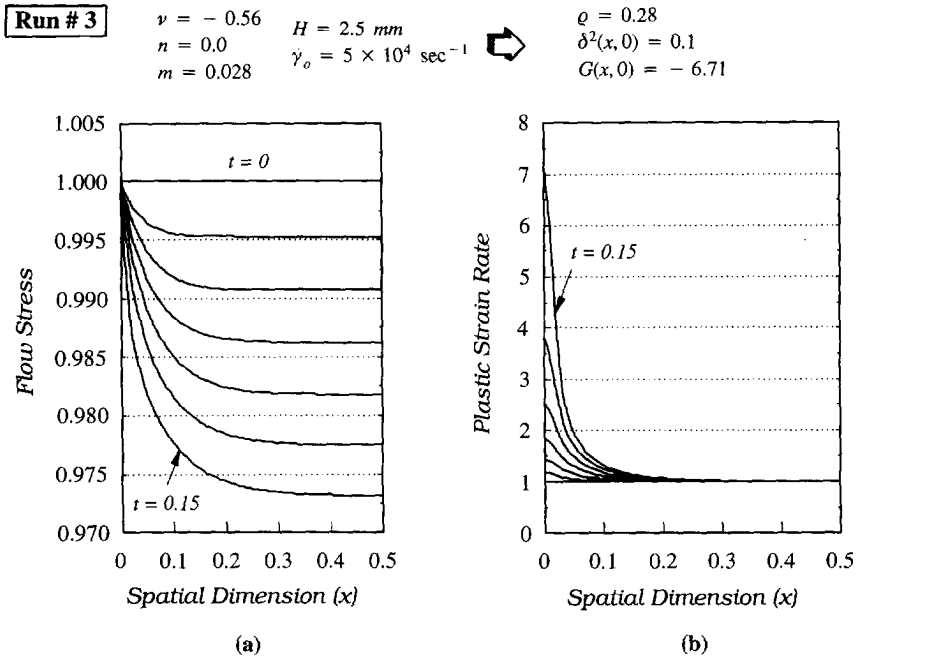

Fig. 13. Spatial evolution of the flow stress and plastic strain rate for run 3.

is attributed to differences in values of δ^2 and G. Based on the initial value of δ^2, the predicted shear band thickness for run 1 is $\delta_1 = 0.42$ while the predicted shear band thickness for run 2 is $\delta_2 = 0.27$. The computed results in Figs 11 and 12 confirm such predictions.

(2) It is important to observe that weaker strain rate sensitivity permits large increases in the plastic strain rate to be associated with very small stress reductions. This can be verified by comparing the results in Figs 11 and 12.

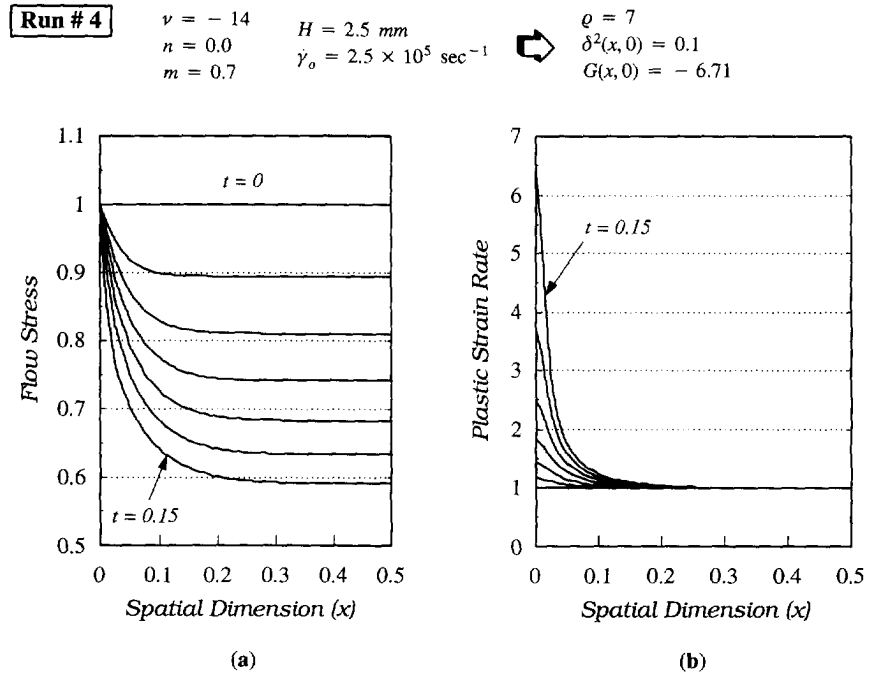

Fig. 14. Spatial evolution of the flow stress and plastic strain rate for run 4.

(3) The test cases labeled run 3 and run 4 are selected so that they have the same values for δ^2 and G. The exponents for the power law in run 4 do not correspond to a real material. They are only selected to emphasize the observation regarding the invariance of the localization response with respect to δ^2 and G.

(4) Examination of the computed results for run 3 and run 4 confirms that the spatial evolution of the plastic strain rate is almost identical for the two cases. On the other hand, the associated stress drop varies significantly for these two runs. This may be qualified by recalling the asymptotic solution (44) which indicates that the outer solution for the flow stress depends primarily on the slope C_p. For the power law model, the flow stress behavior away from the boundaries is expected to be approximated well by

$$\tau(x, t) \approx 1 + tC_p(x, 0). \tag{60}$$

(5) The computed values, at time $t = 0.15$, of the outer flow stress based on eqn (60) are 0.9748, 0.9874, 0.9718, 0.2957 for runs 1–4, respectively. Differences between the foregoing predictions and computed values are attributed to the usage of the initial value of the slope C_p. However, expression (60) appears to provide satisfactory qualitative agreement with the computed results.

(6) Equation (56), based on the solution for a Kelvin–Voigt material, illustrates the dependence of the band strain rate on the values of G. This dependence is numerically verified through the almost identical strain rate response in runs 3 and 4.

9. DISCUSSION: THE DEFORMATION NUMBER AND SHEAR BAND THICKNESS

In this section, we attempt to paint a picture of shear band formation based on conclusions and observations accumulated through the previous sections. Sections 3 and 4 established the connection between the evolution of inhomogeneous, localized plastic flow and the increased importance of inertia for viscoplastic solids with a net softening response subject to the cited conditions. Sections 5 and 6 utilized a model problem to gain further understanding of the aforementioned connection. The interactive roles of material viscosity and inertia were shown to be displayed through the dimensionless group $\delta^2 = S_1/\rho$. Solutions associated with small values of δ^2 were shown to exhibit a boundary layer-like response in which the thickness of the layers scales with $\delta = \sqrt{(S_1/\rho)}$. Section 7 provided an exact solution for the special case of a Kelvin–Voigt material through which we examined the validity of the different frameworks for material stability (Table 1).

In view of the foregoing analyses, we identify the inverse of δ^2 as an important quantity through which the interactive roles of material viscosity and inertia are displayed. We refer to this dimensionless number as the deformation number,

$$R_D \equiv \frac{1}{\delta^2} = \frac{\rho}{S_1}. \tag{61}$$

In terms of *dimensional* values, the above dimensionless group can be expressed as follows:

$$R_D = \frac{\rho V_0^2}{\dot{\gamma}_0^p(\partial\tau/\partial\dot{\gamma})}. \tag{62}$$

Based on the analyses in previous sections, it appears that the deformation number R_D may be used to characterize a deformation as being dynamic or quasi-static rather than relying only on the applied loading rate. Hence, we suggest that large (small) values of the deformation number should be used to characterize a particular deformation as being dynamic (quasi-static). For instance, the deformation corresponding to run 2 is "more dynamic" than that corresponding to run 1 although the loading rate for the two runs is identical. In fact, the deformation numbers are 5.6 and 14 for runs 1 and 2, respectively. In

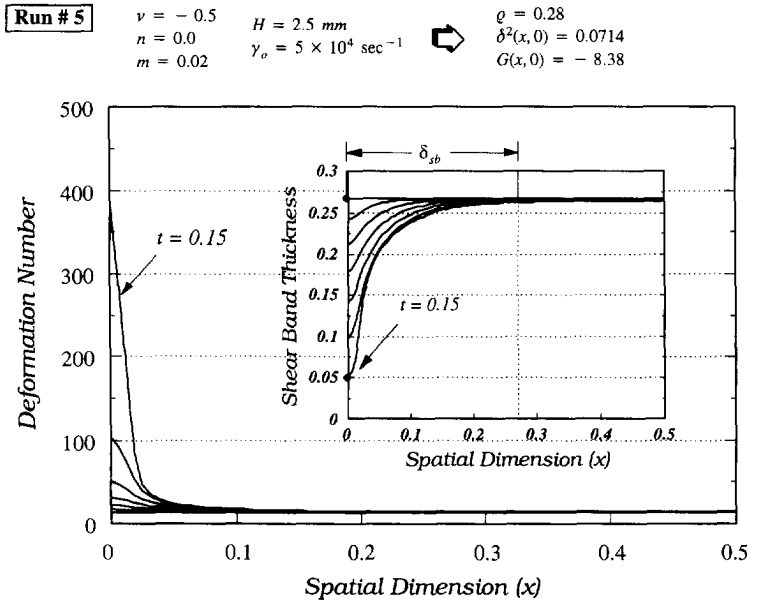

Fig. 15. Spatial evolution of the deformation number $R_D(x, t)$ and shear band thickness $\delta_{sb}(x, t)$ for run 5.

other words, it is the relative strength of inertial to viscous stresses that determines whether a deformation should be viewed as being dynamic or quasi-static.

Furthermore, we recall the asymptotic results of Section 6 as well as the numerical observations of Section 8 which suggest that an upper bound for shear band thickness is given by

$$\delta_{sb} = \frac{1}{\sqrt{(R_D(x,0))}} = \sqrt{\frac{S_1(x,0)}{\rho}}. \tag{63}$$

Specialization of eqn (63) to the power law model while using *dimensional* values renders the following expression for the upper bound of the shear band thickness:

$$\frac{\delta_{sb}}{H} = \sqrt{\left(\frac{m\tau_0}{\rho V_0^2}\right)}. \tag{64}$$

Figure 15 illustrates the spatial evolution of the deformation number $R_D(x, t)$ for run 5 while the insert in Fig. 15 illustrates the spatial evolution of the shear band width $\delta_{sb}(x, t) = 1/[\sqrt{R_D(x, t)}]$ for the same run. Material parameters for run 5 are chosen to simulate the response of a typical structural steel (such as the cold-rolled steel 1018). The large values of the deformation number in the vicinity of the specimen boundary imply the dominance of inertial stresses over viscous stresses. Furthermore, the shaded length in the insert corresponds to the upper bound δ_{sb} computed from expression (64). It is evident that shear band estimates based on expression (64) show excellent agreement with the numerical results for all runs 1–5. It is also interesting to observe that expression (64) can be rewritten as follows:

$$\frac{\delta_{sb}}{H} = \sqrt{\left(\frac{\partial\tau/\partial \ln \dot{\gamma}^p}{\rho V_0^2}\right)}. \tag{65}$$

The term $\partial\tau/\partial \ln \dot{\gamma}^p$ is a logarithmic strain rate sensitivity measure. Examination of expression

(65) implies that localization of the deformation in a narrow region of width $\delta_{sb} \ll H$ requires that

$$\rho V_0^2 \gg \frac{\partial \tau}{\partial \ln \dot{\gamma}^p}, \tag{66}$$

i.e. the kinetic energy associated with this deformation should be much larger than the material viscosity (as expressed by the foregoing logarithmic measure). The reader is referred to the articles by Cherukuri and Shawki (1995a,b) in which a similar connection between flow localization and system kinetic energy is established for the case of velocity-controlled boundaries.

Finally, we note that expression (63) shows no dependence on initial imperfections. It is also important to note that expression (63) provides us with the following limiting cases:

$$\delta_{sb} \to 0 \quad \text{as} \quad S_1 \to 0, \quad (\rho \neq 0), \tag{67a}$$

$$\delta_{sb} \to \infty \quad \text{as} \quad \rho \to 0, \quad (S_1 \neq 0). \tag{67b}$$

The limit (67a) corresponds to dynamic deformations of rate-independent materials ($R_D \to \infty$) whereas expression (67b) corresponds to quasi-static deformations of viscoplastic materials ($R_D \to 0$). The interactive roles of material viscosity and inertia regarding the introduction of a length scale to this problem are evident.

Acknowledgements The support of the National Science Foundation through grant No. NSF MSM 87-09299 and the Presidential Young Investigator Award No. NSF MSS 89-57180 is gratefully acknowledged. Calculations were performed on the HP 9000, Model 755 and a NeXT TurboStation which were made possible through partial donations from the Hewlett Packard Company, the NeXT Computer Company and matching funds from the National Science Foundation.

REFERENCES

Cherukuri, H. P. and Shawki, T. G. (1995a). *Int. J. Plasticity* **11,** 15.
Cherukuri, H. P. and Shawki, T. G. (1995b). *Int. J. Plasticity* **11,** 41.
Coddington, E. A. and Levinson, N. (1955). *Theory of Ordinary Differential Equations*. McGraw-Hill, New York.
Molinari, A. and Clifton, R. J. (1983). Private communication.
Molinari, A. and Clifton, R. J. (1988). *J. Appl. Mech.* **54,** 806.
Nayfeh, A. (1973). *Perturbation Methods*. John Wiley and Sons.
Rice, J. R. (1977). *Proceedings of the 14th IUTAM Congress*, Delft, The Netherlands, p. 207. North-Holland, Amsterdam.
Rudnicki, J. W. and Rice, J. R. (1975). *J. Mech. Phys. Solids* **23,** 371.
Shawki, T. G. and Clifton, R. J. (1989). *Mech. Mater.* **8,** 13.
Wu, F. H. and Freund, L. B. (1984). *J. Mech. Phys. Solids* **32,** 119.